Spatial Resonances and Superposition Patterns in a Reaction-Diffusion Model with Interacting Turing Modes

Lingfa Yang, Milos Dolnik, Anatol M. Zhabotinsky, and Irving R. Epstein*

Department of Chemistry and Center for Complex Systems, MS 015, Brandeis University, Waltham, Massachusetts 02454-9110

(Received 13 November 2001; published 6 May 2002)

Spatial resonances leading to superlattice hexagonal patterns, known as "black-eyes," and superposition patterns combining stripes and/or spots are studied in a reaction-diffusion model of two interacting Turing modes with different wavelengths. A three-phase oscillatory interlacing hexagonal lattice pattern is also found, and its appearance is attributed to resonance between a Turing mode and its subharmonic.

DOI: 10.1103/PhysRevLett.88.208303 PACS numbers: 82.40.Bj, 47.54.+r, 82.20.–w, 89.75.Kd

Resonance phenomena often occur when a nonlinear pendulum is subjected to periodic forcing, becoming entrained at a frequency that is rationally related to the applied frequency [1]. The "pendulum" can be a physical oscillator, a chemical system such as the Belousov-Zhabotinsky reaction [2], or even a biological oscillator. Depending on the source of the forcing, the resonance can be classified as either external or internal. Resonance is generally thought of as being associated with temporal oscillations, but it can also arise when a periodic spatial pattern is subjected to spatial forcing.

Reaction-diffusion systems can produce Turing patterns [3], which are stationary in time and periodic in space. Most experimental studies of Turing patterns [4–6] have explored structures with a single characteristic wavelength. An interesting exception is the black-eye pattern, interpreted as a resonance between two hexagonal lattices [7].

In many systems, a Turing instability interacts with a Hopf instability, a phenomenon explored in the Brusselator [8], in a semiconductor model [9], and in the Lengyel-Epstein model [10]. However, with the exception of a single recent study of a bistable system [11], the problem of interaction between Turing modes has been neglected, despite experimental evidence [7,12] of superposition patterns that may arise from such interactions. Natural patterns such as fish skins [13] and morphogenetic phenomena [14] provide examples of superlattice patterns with more than one wavelength. Superlattice patterns have been found in an equivariant bifurcation analysis of reaction-diffusion models [15], where the mechanism for complex pattern formation involves interactions between modes of equal wave number and different spatial phase. Black-eye patterns have been observed experimentally in optical systems with a spatial Fourier filter in a feedback loop [16].

Black-eye patterns were first seen in a reaction-diffusion experiment involving the chlorite-iodide-malonic acid (CIMA) reaction in a thin layer gel reactor [7]. A subsequent study [17] suggested that black-eye patterns are not two-dimensional, but rather projections of a three-dimensional body-centered cubic lattice. Recent experimental results suggest that the three-dimensional interpretation is not appropriate [18], but until now no model has been developed that reproduces the black-eye patterns in two dimensions. Here we propose a model that generates not only black-eye patterns but also a variety of other spatial resonant patterns that result from interactions between different Turing modes, or between a single mode and its harmonics.

In order to construct a model with two interacting Turing modes, we linearly couple two systems, each possessing a single Turing mode. Physically, such a model might represent two thin layers of gel that meet at an interface. Each layer contains the same set of reactants with the same kinetics; the difference between the layers arises from differential diffusion due to physical (density or viscosity) or/and chemical (complex formation) factors. The layer with faster diffusion gives rise to the longer wavelength Turing mode.

The interaction between two such coupled layers can be described by a set of partial differential equations:

$$\begin{aligned} \frac{\partial x_i}{\partial t} &= D_{x_i}\nabla^2 x_i + \alpha(x_j - x_i) + f(x_i, y_i), \\ \frac{\partial y_i}{\partial t} &= D_{y_i}\nabla^2 y_i + \beta(y_j - y_i) + g(x_i, y_i), \end{aligned} \tag{1}$$

where the reactive species, x and y, and their diffusion coefficients, D_x and D_y, are distinguished by subscripts $i, j = 1, 2, i \neq j$ that specify which layer they are in. The Laplacian terms describe two-dimensional diffusion in the (horizontal) plane of the interface, while vertical diffusion between the layers is represented by the linear coupling terms involving the parameters α and β. The functions f and g specify the kinetic behavior of the system.

We present here results for the Brusselator model [19], whose kinetics are given by $f(x, y) = a - (1 + b)x + x^2y$, and $g(x, y) = bx - x^2y$. We performed a series of two-dimensional simulations; in each, the initial condition was a small random perturbation of the uniform steady state. When the system reached a stable state (stationary or oscillatory), we took a snapshot showing gray levels linearly proportional to x_1, with white (black) corresponding to high (low) concentration. Unless otherwise specified, the physical size of the system was 200×200 space

units. Periodic boundary conditions were employed in all cases. The dominant mode (long wavelength) was fixed at $k_1 = 0.2$, while the secondary mode (short wavelength) was located at various values of k to study the resulting resonance behavior or superposition patterns. The parameter values used in our simulations are given in Table I.

To study the resonant behavior, we set the $\mathrm{Re}(\lambda)$ maximum at $(k_1, h_1) = (0.2, 0.1)$, and set $h_2 = -0.2$ for the secondary Turing mode (Fig. 1) [20]. Thus, the wave number k_2 served as our control parameter. If we vary r to maintain both modes near onset, we obtain resonant behavior at both weak ($\alpha = 0.1$) and strong ($\alpha = 1.0$) coupling, since the wave numbers at onset depend only weakly on the coupling. As the ratio k_2:k_1 was varied, we observed clear evidence of phase-locking behavior near 2:1 and 3:1, with black-eye and white-eye patterns, respectively (Fig. 2).

The black-eye patterns can be understood as a resonance between two hexagonal lattices. The major modes, as wave vectors, can be recognized from the two-dimensional Fourier spectra (lower panels in Fig. 2). Figure 2b displays a resonance around $\sqrt{3}$:1. This type of black-eye pattern is the same as that reported in the CIMA reaction [7] and in optical systems [16]. Figure 2c shows another type of black-eye pattern, where the resonance is located around 2:1. Switching between these two types was found to be continuous.

In black-eye patterns, the center is black (low concentration) and is surrounded by a white (high concentration) ring, with these eyelike spots arranged in a hexagonal lattice. The patterns found near a 3:1 wavelength ratio show a "white-eye" [21] pattern (Fig. 2d). The center is white, surrounded by a black ring and a white ring.

The parameters used in Fig. 2 (see Table I) represent weak coupling. Stronger coupling makes the separation between the two modes shallower, but does not change the characteristic wavelength and has no significant influence on the resonance behavior. Both black-eye and white-eye patterns were also obtained at stronger coupling ($\alpha = 1.0$).

The resonant behavior we have found in the Brusselator appears to be generic for systems with two coexisting Turing modes. For example, in the Lengyel-Epstein model of the CIMA reaction [22], the kinetics are given by $f(x, y) = a - \frac{4xy}{1+x^2}$, and $g(x, y) = b[x - \frac{xy}{1+x^2}]$. With parameters $(a, b) = (15, 9)$, $\alpha = \beta = 0.1$, and diffusion coefficients $D = (6, 80, 23, 380)$, simulations yielded the same type of resonant patterns as described above.

A black-eye pattern can be decomposed into a linear combination of the fundamental mode and superharmonic modes of the underlying hexagonal lattice. The contribution of each mode can be retrieved from the spot density in the power spectrum. Suppose that v_0, v_1, and v_2 denote hexagonal lattices with wave numbers $k = 1, \sqrt{3}$, and 2, respectively, which can be expressed as Neumann series [16]:

$$v_n(\mathbf{r}) = \sum_{j=1}^{6} \exp[i\mathbf{q}_n^j \cdot \mathbf{r}], \qquad n = 0, 1, 2, \qquad (2)$$

where $\mathbf{q}_0, \mathbf{q}_1$, and $\mathbf{q}_2$ are wave vectors, as illustrated in the Fourier spectra in Fig. 2. The black-eye pattern in Fig. 2b can be reconstructed as $v = \frac{1}{8}v_0 - \frac{5}{8}v_1 - \frac{1}{4}v_2$, while that in Fig. 2c is given by $v = \frac{1}{8}v_0 - \frac{1}{4}v_1 - \frac{5}{8}v_2$. The white-eye pattern in Fig. 2d can be reconstructed in the same fashion if higher order resonant wave vectors are included.

The patterns described above arise from an internal spatial resonance, which requires three conditions: (i) The ratio of wavelengths of the two modes is close to 2:1, 3:1, or $\sqrt{3}$:1; (ii) the two modes must have the same symmetry, e.g., hexagonal; and (iii) the maxima of $\mathrm{Re}(\lambda)$ lie within the ranges $0 < h_1 < 0.3$, and $-0.5 < h_2 < 0$. If these conditions are not satisfied, there is no resonance, and superposition patterns or single wavelength Turing patterns are formed.

Figure 3 shows four different types of superposition patterns. Each has two characteristic wavelengths (the major peaks in the two-dimensional power spectrum fall on two distinct circles). The longer wavelength Turing pattern can be stripelike (Figs. 3a and 3b) or hexagon (spot) like (Figs. 3c and 3d). The shorter wavelength pattern can be composed of stripes (Fig. 3d) or of white (Figs. 3b and 3c) or black (Fig. 3a) spots. These patterns do not exhibit resonant behavior, because each of them violates at least one of the above requirements.

TABLE I. Parameters used in simulations of model (1) with Brusselator kinetics ($\alpha = \beta$).

Figure	a	b	α	D_{x_1}	D_{y_1}	D_{x_2}	D_{y_2}	k_1	h_1	k_2	h_2
1	3	9	1	5	14	54.9	159.8	0.2	0.2	0.6	−0.2
2b	3	9	0.1	16.7	36.4	49.5	117.6	0.2	0.1	0.35	−0.2
2c	3	9	0.1	12.6	27.5	49.4	117.6	0.2	0.1	0.4	−0.2
2d	3	9	0.1	5.60	12.3	49.3	117.5	0.2	0.1	0.6	−0.2
3a	3	9	0.1	12.6	27.5	47.5	141.5	0.2	0.8	0.4	−0.2
3b	3	9	1	1.85	5.66	50.6	186.0	0.2	0.8	1	0
3c	3	6	1	1.31	9.87	34.0	344.9	0.2	0.8	1	0
3d	3	10	1	2.03	4.38	56.2	135.3	0.2	0.2	1	−0.5
4	3	9.9	1	8.33	8.33	46.0	120.0	0.2	0.1	⋯	⋯

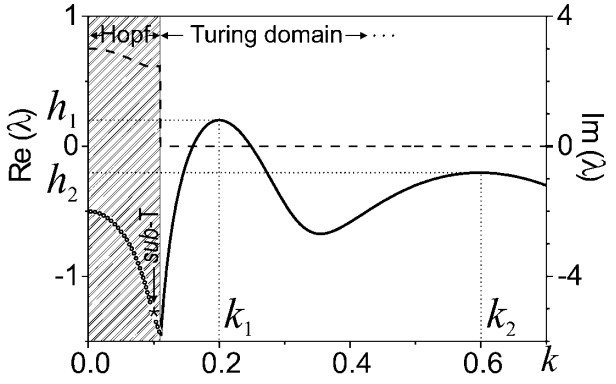

FIG. 1. Typical dispersion curve for model (1). Solid line: real part of dominant eigenvalue; dashed line: imaginary part. Hopf (shadow) and Turing domains refer to regions where the most positive eigenvalue has nonzero and zero imaginary parts, respectively. Turing modes located at (k_1, h_1), and (k_2, h_2).

The pattern shown in Fig. 3a has a wavelength ratio of exactly 2:1, but fails to show resonance because it violates symmetry matching. Stability analysis shows that the first Turing mode in this case lies far above the onset point, which results in a striped Turing pattern. The second mode produces black spots, and the interaction between them causes the spots to arrange themselves along the stripes (Fig. 3a). The stripe-spot patterns in Figs. 3b and 3d also violate symmetry matching.

All the patterns in Figs. 3b–3d show superpositions rather than resonance, because the wavelength ratio is much larger (5:1) than one of the aforementioned resonant ratios.

The resonances examined above are superharmonic resonances, where the basic mode resonates with modes at higher wave numbers. Subharmonic resonances, involving secondary modes with lower wave numbers, also arise in our model. The fundamental Turing mode has $(k_1, h_1) = (0.2, 0.3)$, which gives rise to a hexagonal lattice. Its spatial subharmonic mode (sub-T) has wave number $k_{\text{sub}} = k_1/\sqrt{3} = 0.12$, and lies within the Hopf domain (Fig. 1). The existence of sub-T, with $\omega \neq 0$, results in the development of a temporally oscillating subhexagonal lattice. This oscillation breaks the D_6 symmetry of the original lattice, which degenerates to the subgroup D_3. The hexagonal array of spots thus separates into three sets, each forming a hexagonal sublattice with wavelength $\sqrt{3}$ times the wavelength of the original lattice and shifted in phase by $\frac{2}{3}\pi$ from the other sublattices (Fig. 4).

Each type of spot falls into one hexagonal sublattice (Fig. 4a). In the absence of defects, the three sublattices are interlaced as shown in Fig. 4b. The striking manner in which each spot in the pattern cycles through the three manifestations shown in Fig. 4a—black, gray, and white-circled—leads us to dub this new resonance a "twinkling-eye" pattern.

Twinkling-eye patterns are found when the basic Turing mode lies just above the onset point and sub-T is also close to onset but within the Hopf domain. When the basic mode is too far above onset, the Turing pattern is striped. The stripes themselves do not move, but their midlines serve as sinks (or as sources if half a period away)

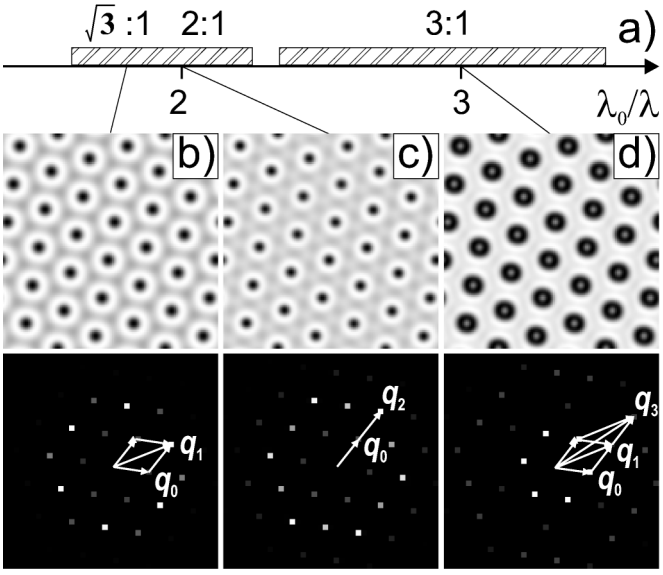

FIG. 2. Internal spatial resonance and typical resonant patterns. Upper panels: (a) phase-locking range; (b) black-eye pattern near $\sqrt{3}$:1; (c) black-eye pattern near 2:1; (d) white-eye pattern near 3:1. Corresponding Fourier spectra (lower panels) show basic mode and superharmonic modes of hexagonal lattices; arrows $\mathbf{q}_0, \mathbf{q}_1, \mathbf{q}_2$, and $\mathbf{q}_3$ are wave vectors pointing to typical modes.

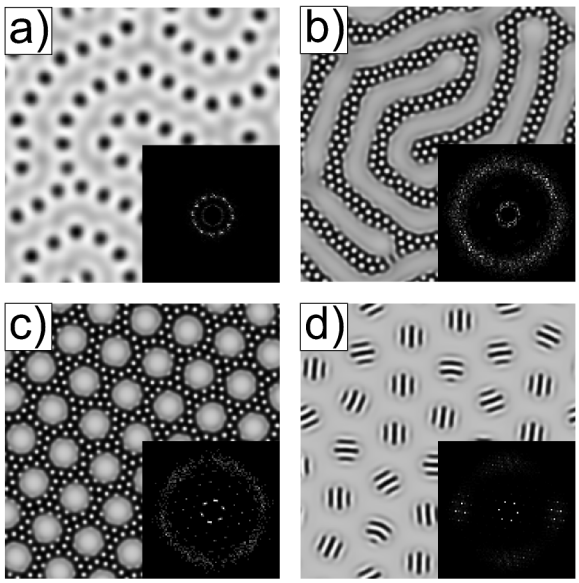

FIG. 3. Superposition patterns: (a) black dots on long stripes; (b) small white dots on stripes; (c) small white dots on background of large hexagons; (d) short thin stripes on hexagonal array of spots.

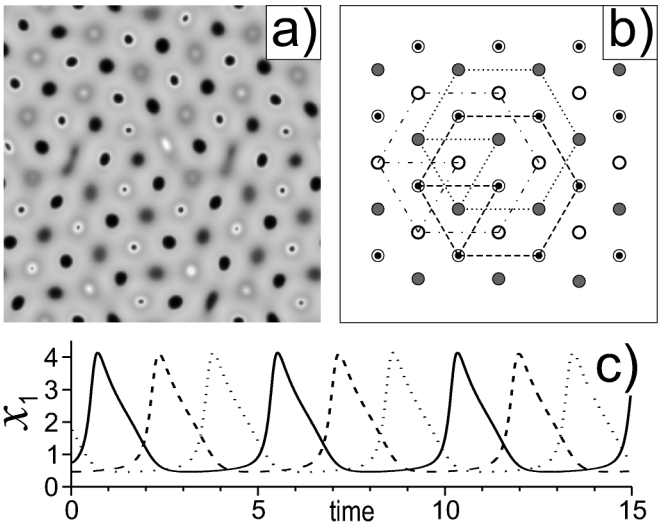

FIG. 4. Twinkling-eye pattern: (a) single snapshot, 300 × 300 space units; (b) the three hexagonal sublattices indicated by empty circles, filled circles, and dot-center circles; (c) three-phase oscillations (solid, dashed, and dotted lines) at center points of eyes in the three sublattices. Phase shift: $\frac{2}{3}\pi$; period: 4.8 time units.

of the localized traveling waves that arise from the Hopf instability. Such patterns have been reported to arise from subharmonic Turing-Hopf interaction [23].

The black-eye, white-eye, and superposition patterns described here are generic in that they arise from the interaction of unstable spatial modes with appropriate ratios of wave numbers. Similar resonant patterns are found in experiments on optical systems [16] and with periodic spatial (external) forcing of Turing structures [24], and can be obtained by analysis of general amplitude equations near a bifurcation point [15,25]. The twinkling-eye pattern, on the other hand, requires interaction between a Turing mode and its subharmonic located within an oscillatory Hopf domain, a situation less likely to occur generically. While these complex behaviors can occur in other types of systems, particularly when they are subject to spatial forcing, we expect them to be most common in reaction-diffusion systems, where the possibility of species diffusing at significantly different rates can give rise to multiple, potentially resonant, length scales.

This work was supported by the Chemistry Division of the National Science Foundation.

*To whom correspondence should be addressed.

[1] *Nonlinear Dynamics and Chaos,* edited by J. M. T. Thompson and H. B. Stewart (Wiley, Chichester, 1986).
[2] V. Petrov, Q. Ouyang, and H. L. Swinney, Nature (London) **388**, 655 (1997).
[3] A. M. Turing, Philos. Trans. R. Soc. London B **237**, 37 (1952).
[4] V. Castets, E. Dulos, J. Boissonade, and P. De Kepper, Phys. Rev. Lett. **64**, 2953 (1990).
[5] Q. Ouyang and H. L. Swinney, Nature (London) **352**, 610 (1991).
[6] I. Lengyel, S. Kadar, and I. R. Epstein, Phys. Rev. Lett. **69**, 2729 (1992).
[7] G. H. Gunaratne, Q. Ouyang, and H. L. Swinney, Phys. Rev. E **50**, 2802 (1994).
[8] J.-J. Perraud, A. De Wit, E. Dulos, P. De Kepper, G. Dewel, and P. Borckmans, Phys. Rev. Lett. **71**, 1272 (1993); A. De Wit, D. Lima, G. Dewel, and P. Borckmans, Phys. Rev. E **54**, 261 (1996).
[9] S. Bose, P. Rodin, and E. Schöll, Phys. Rev. E **62**, 1778 (2000).
[10] A. Rovinsky and M. Menzinger, Phys. Rev. A **46**, 6315 (1992).
[11] G. Dewel, M. Bachir, S. Metens, and P. Borckmans, Faraday Discuss. **120**, 421 (2001).
[12] J. Boissonade, E. Dulos, and P. De Kepper, in *Chemical Waves and Patterns,* edited by R. Kapral and K. Showalter (Kluwer, Dordrecht, 1995), p. 221.
[13] R. A. Barrio, C. Varea, J. L. Aragon, and P. K. Maini, Bull. Math. Biol. **61**, 483 (1999).
[14] P. K. Maini, K. J. Painter, and H. N. P. Chau, J. Chem. Soc. Faraday Trans. **93**, 3601 (1999).
[15] S. L. Judd and M. Silber, Physica (Amsterdam) **136D**, 45 (2000).
[16] M. A. Vorontsov and B. A. Samson, Phys. Rev. A **57**, 3040 (1998).
[17] M. G. Gomes, Phys. Rev. E **60**, 3741 (1999).
[18] C. Zhou, H. Guo, and Q. Ouyang, Phys. Rev. E **65**, 036118 (2002).
[19] I. Prigogine and R. Lefever, J. Chem. Phys. **48**, 1695 (1968).
[20] We set $h_1 > h_2$ and choose h_1 just above onset in order to obtain the desired hexagonal pattern. Even when the secondary maximum in the dispersion curve lies slightly below the real axis, the corresponding mode can interact nonlinearly with the basic mode and contribute to stable pattern formation. If h_1 is too high, striped patterns arise; if $h_2 > h_1$, the second mode becomes dominant.
[21] White-eye patterns have been found in experiments by O. Steinbock, E. Kasper, and S. C. Müller, J. Phys. Chem. A **103**, 3442 (1999).
[22] I. Lengyel and I. R. Epstein, Science **251**, 650 (1991).
[23] A. De Wit, Adv. Chem. Phys. **109**, 435 (1999).
[24] M. Dolnik, I. Berenstein, A. M. Zhabotinsky, and I. R. Epstein, Phys. Rev. Lett. **87**, 238301 (2001).
[25] *Spatio-temporal Pattern Formation: With Examples From Physics, Chemistry, and Materials Science,* edited by D. Walgraef (Springer, New York, 1997).